Electronic Supplementary Material (ESI) for Journal of Materials Chemistry C.

Triphenylamine-Based Pt(II) Metallacage via Coordination-Driven Self-Assembly for Nonlinear Optical Power Limiting

Zihao Yin, Xingmao Chang, Jianyang Zang, Simin Lin, Zhijie Zhou, Taihong Liu, Liping Ding, Haonan Peng,* and Yu Fang

Key Laboratory of Applied Surface and Colloid Chemistry (Ministry of Education), School of Chemistry and Chemical Engineering, Shaanxi Normal University, Xi'an 710062, P. R. China

*Corresponding authors: phn@snnu.edu.cn

Contents

1. Synthesis details of the compounds

1.1 Synthesis of *cis*-$(PEt_3)_2Pt(OTf)_2$

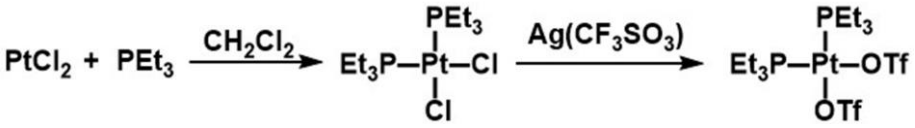

To a 200 mL Schlenk bottle wrapped with aluminum foil were added $PtCl_2$ (3.3 g, 12.4 mmol), and then added 80 mL anhydrous dichloromethane to dissolve it. Following 25 mL PEt_3(25.0 g, 20 wt% in ethanol solution, 42.3 mmol) was added. The mixture was stirred in dark at room temperature for 6 days. Then the solvent was evaporated and the residue is recrystallized by CH_2Cl_2/CH_3OH to get white solid, the solid was washed by CH_3OH to get the $PtCl_2(PEt_3)_2$. Yield: 45%. ^{1}H NMR (600 MHz, CD_2Cl_2, 298 K) δ (ppm): 2.09-1.97 (m, 12H), 1.22-1.07 (m, 18H). $^{31}P\{^1H\}$ NMR (243 MHz, CD_2Cl_2, 298 K) δ (ppm): 9.00 (^{195}Pt satellites, $^1J_{Pt-P}$ = 3509.2 Hz).

$PtCl_2(PEt_3)_2$ (500.0 mg, 1.0 mmol) and $Ag(CF_3SO_3)$ (524.3 mg, 2.04 mmol) were dissolved in 10 mL CH_2Cl_2, and the mixture was stirred in dark at room temperature for 8 h. Afterwards the solution was filtered, and the solvent was removed by nitrogen flow. The solid was dissolved in 1 mL CH_2Cl_2 and then added 9 mL ethyl ether to get precipitate, the final product was collected by centrifugation to give *cis*-$(PEt_3)_2Pt(OTf)_2$ as a gray-white solid. Yield: 95 %. ^{1}H NMR (600 MHz, CD_2Cl_2, 298 K) δ (ppm): 2.05-1.84 (m, 12H), 1.34-1.16 (m, 18H). $^{31}P\{^1H\}$ NMR (243 MHz, CD_2Cl_2, 298 K) δ (ppm): 8.93 (^{195}Pt satellites, $^1J_{Pt-P}$ = 3772.6 Hz).

1.2 Synthesis of the ligand

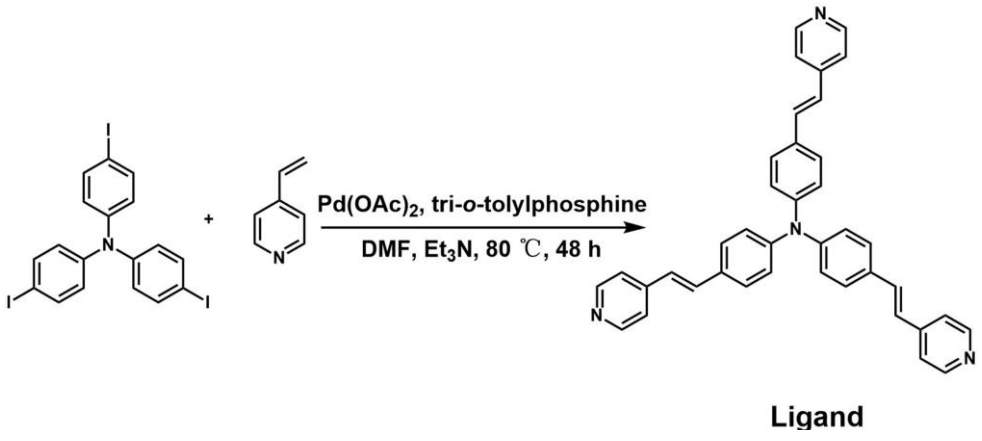

Ligand

Yield: 55 %. ^{1}H NMR (600 MHz, CD_2Cl_2, 298 K) δ (ppm): 8.53 (d, *J* = 6.0 Hz, 6H), 7.50 (d, *J* = 8.6 Hz, 6H), 7.37 (d, *J* = 6.0 Hz, 6H), 7.32 (d, *J* = 16.3 Hz, 3H), 7.14 (d, *J* = 8.6 Hz, 6H), 6.98 (d, *J* = 16.3 Hz, 3H). ^{13}C NMR (151 MHz, CD_2Cl_2, 298 K) δ (ppm): 150.01 (s), 147.34 (s), 144.77 (s), 132.29 (s), 131.41 (s), 128.12 (s), 124.71 (s), 124.36 (s), 120.60 (s).

1.3 Synthesis of the metallacage

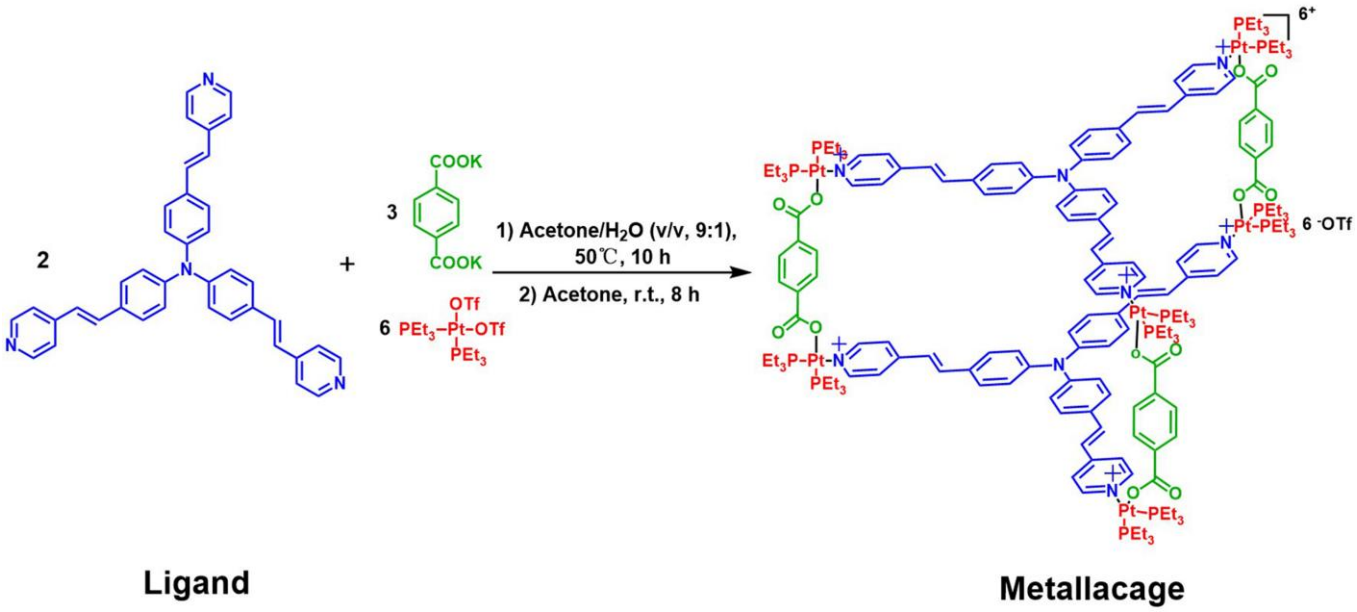

Yield: 92 %. ^{1}H NMR (600 MHz, CD_2Cl_2, 298 K) δ (ppm): 8.57 (d, *J* = 3.5 Hz, 12H), 7.72 (s, 12H), 7.55 (d, *J* = 6.1 Hz, 12H), 7.47 (d, *J* = 8.7 Hz, 12H), 7.41 (d, *J* = 16.2 Hz, 6H), 7.03 (d, *J* = 8.6 Hz, 12H), 6.91(d, *J* = 16.3 Hz, 6H). ^{31}P{^{1}H} NMR (243 MHz, CD_2Cl_2, 298 K) δ (ppm): 4.72 (d, $^{2}J_{P\text{-}P}$ = 21.6 Hz, ^{195}Pt satellites, $^{1}J_{Pt-P}$ = 3152.0 Hz), and - 0.60 (d, $^{2}J_{P\text{-}P}$ = 21.4 Hz, ^{195}Pt satellites, $^{1}J_{Pt-P}$ = 3556.5 Hz). ESI-TOF-MS: m/z 1545.41 ([M-3OTf]$^{3+}$) and 1122.07 ([M-4OTf]$^{4+}$).

2. Details for the Two-Photon Absorption (2PA) and OPL Measurements

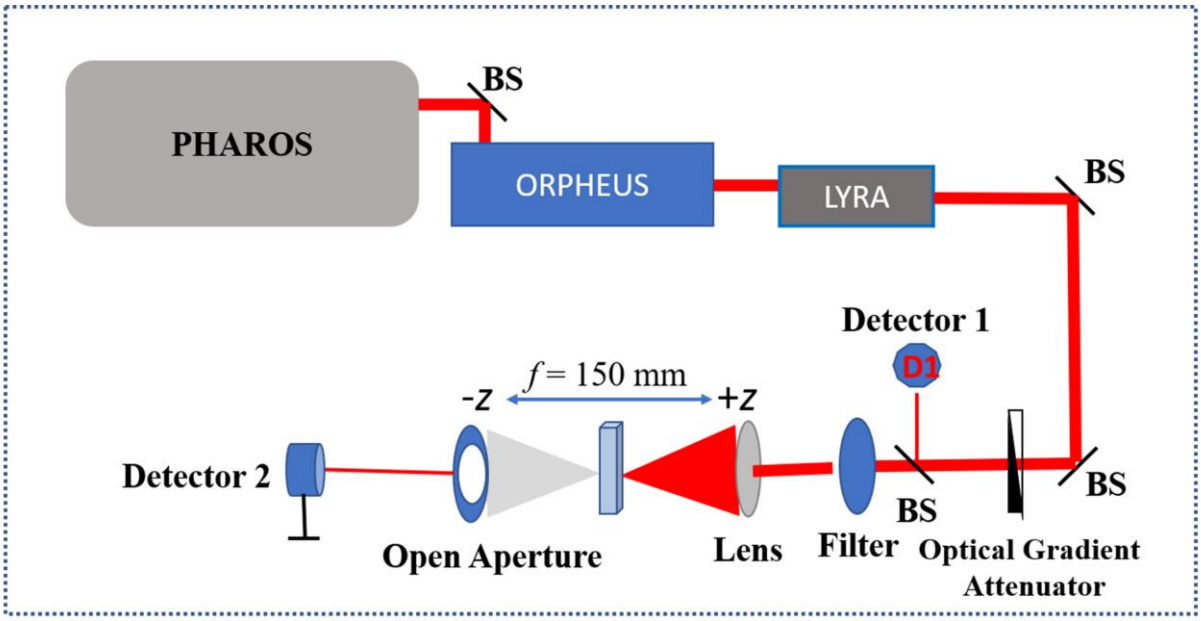

Scheme S1. Schematic diagram of femtosecond open-aperture Z-scan set-up in 2PA measurements.

The single wavelength Z-scan technique is widely used to determine 2PA cross-section (δ_{2PA}) due to its simplicity and accuracy. The experimental setup for femtosecond Z-scan absorption measurements has been widely described elsewhere and shown in Scheme S1.[1,2] In this work, δ_{2PA} values were obtained for the specific wavelength delivered by the source with femtosecond pulses of kHz repetition rate. Measurements of the δ_{2PA} values were performed by the open aperture Z-scan technique focused on the 630-1000 nm spectral region. In detail, the laser source was a mode-locked Yb:KGW laser (Light Conversion, Pharos) with a pulse width of 200 fs and a repetition rate of 10 kHz. An output of 1028 nm was converted using an optical parametric amplifier (Light Conversion, Orpheus) as well as a second harmonic generator (Light Conversion, Lyra), which could be manually tuned to produce radiation ranging from 315 nm to 2600 nm. Using a lens system, the collection was focused on a PM320E photodiode (Thorlabs) with 150 mm long travel stages (Thorlabs). The pulses were focused onto a cuvette filled with the sample, where it produced GW-level intensity at the focal point of the lens and the laser input was high enough for the purpose of 2PA measurements. The sample concentrations were 1.0×10^{-2} M and 2.0×10^{-3} M. Sample cuvette with 1.0 mm length satisfied the condition that the cell-length was less than the Rayleigh range. Neutral density filters were utilized for attenuating the input pulse energy. Using the open aperture Z-scan configuration, the nonlinear absorption coefficient (β) of the sample was measured. Each measurement was repeated

multiple times and averaged to retrieve the NLO coefficients.[3,4] The OPL measurements were performed on the same femtosecond laser system using 1 mm path length quartz cuvettes with dye concentrations ~ 1.0×10^{-2} M. To scan the sample in closed aperture configuration simultaneously, a variable aperture was placed in front of the photodetector in an additional path. The closed aperture Z-scan data provided the sign and magnitude of the nonlinear refractive index (n_2 or r).[1,5,6]

PHAROS laser system employs a chirped pulse amplification technique, which is based on stretching the seed pulses, amplification and compression to achieve the highest pulse peak power with an ultrashort pulse duration. In which the oscillator is made from a single monolithic aluminum block that ensures stable operation. The oscillator comprises chirped mirrors for group velocity dispersion compensation. Yb:KGW is used as a gain medium, directly pumped by laser diode modules. The repetition rate of the oscillator pulses is typically 76 MHz with an average power ranging from 0.6 to 2 W. Spectral bandwidth is within 10-25 nm (FWHM) and yields a corresponding pulse duration of ~70-90 fs. The resulting pulse width can be tuned by changing the compressor length. Tuning the pulse duration is accomplished by inducing positive or negative chirp from a model-specific shortest value to a maximum of approximately 10 ps.

3. Linear photophysical properties

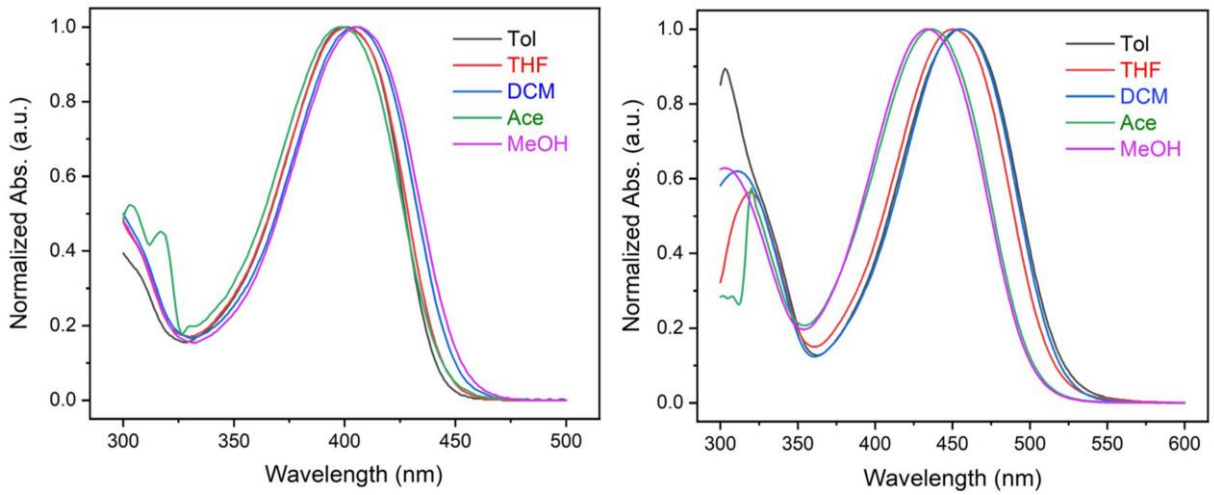

Figure S1. UV−vis absorption spectra of the ligand (left) and the metallacage (right) in different solvents (c = 1 × 10^{-5} M, λ_{ex} = 400/430 nm). Tol: toluene; THF: tetrahydrofuran; DCM: dichloromethane; Ace: acetone; MeOH: methanol.

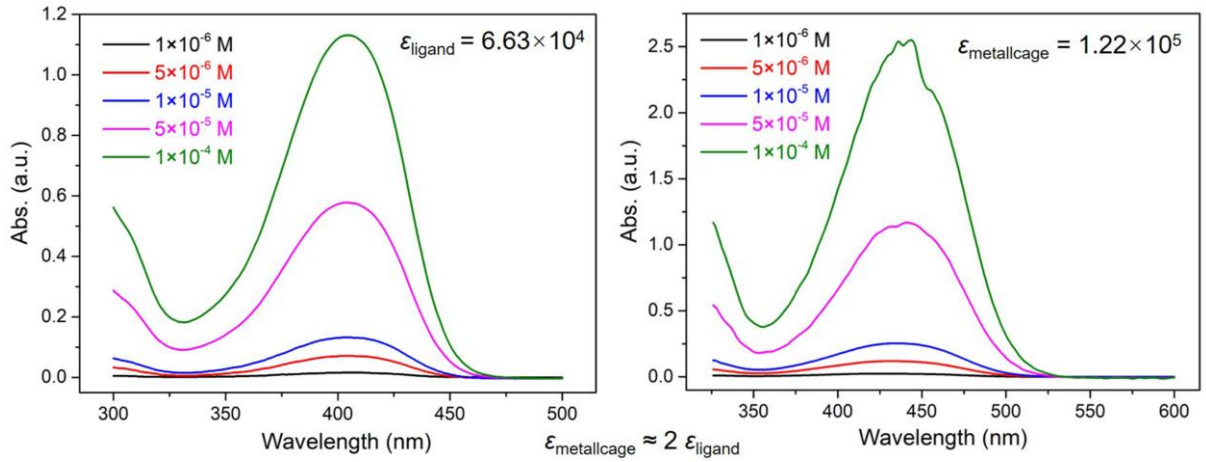

Figure S2. UV−vis absorption spectra of the ligand (left) and the metallacage (right) at different concentrations in DMF. ε is the molar extinction coefficients of the compound.

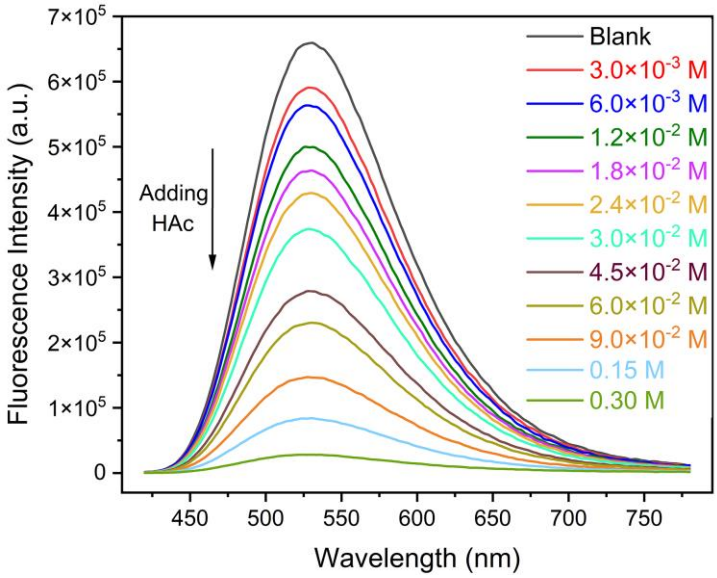

Figure S3. Spectral changes of the fluorescence emission of the 1×10^{-5} ligand in acetone with gradual adding HAc.

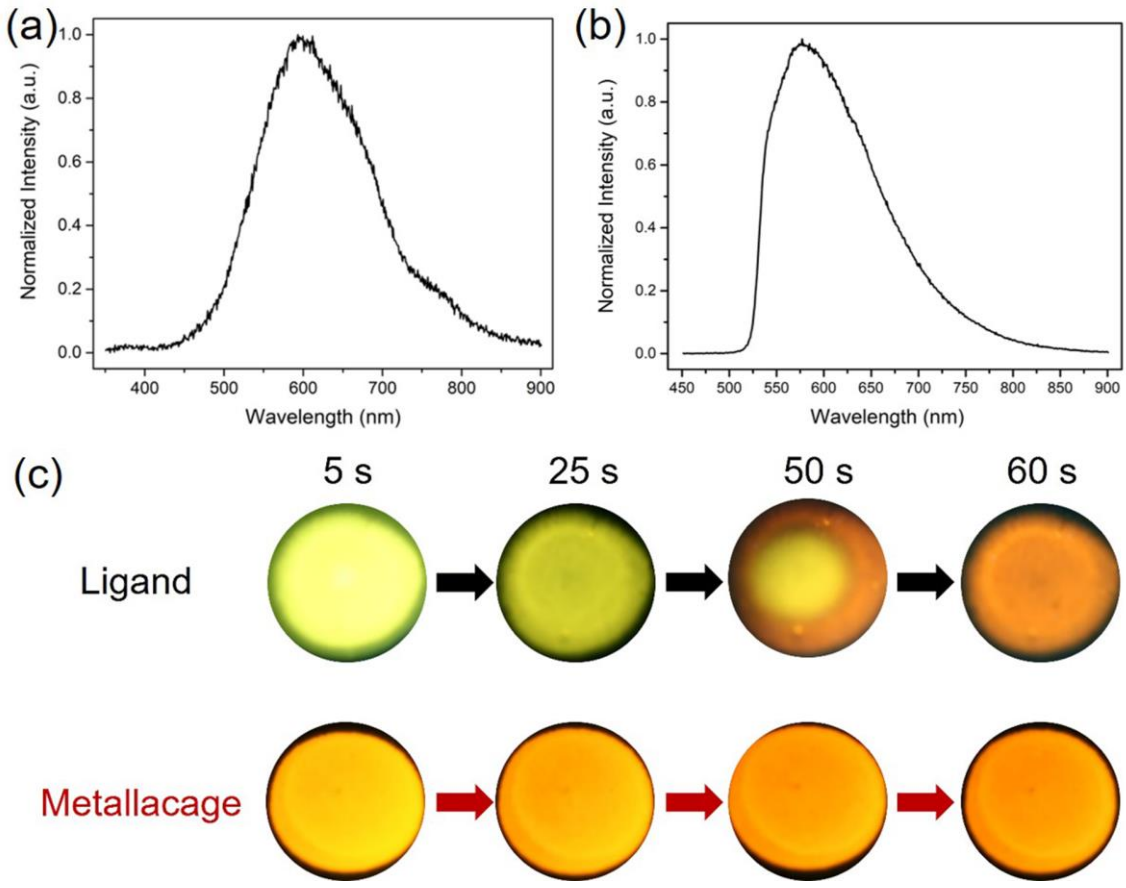

Figure S4. Fluorescence emission spectra of the ligand (a) and the metallacage (b) in film state with a silica gel plate as the substrate, the excitation wavelength is 400 nm. (c) The photographs of the fluorescence change of the ligand and the metallacage in film state when exposed in air for 1 min. The photos were taken under UV light (365 nm) illumination. The fluorescence of the ligand changes significantly within one minute is due to that the ligand gradually aggregates with the evaporation of the solvent.

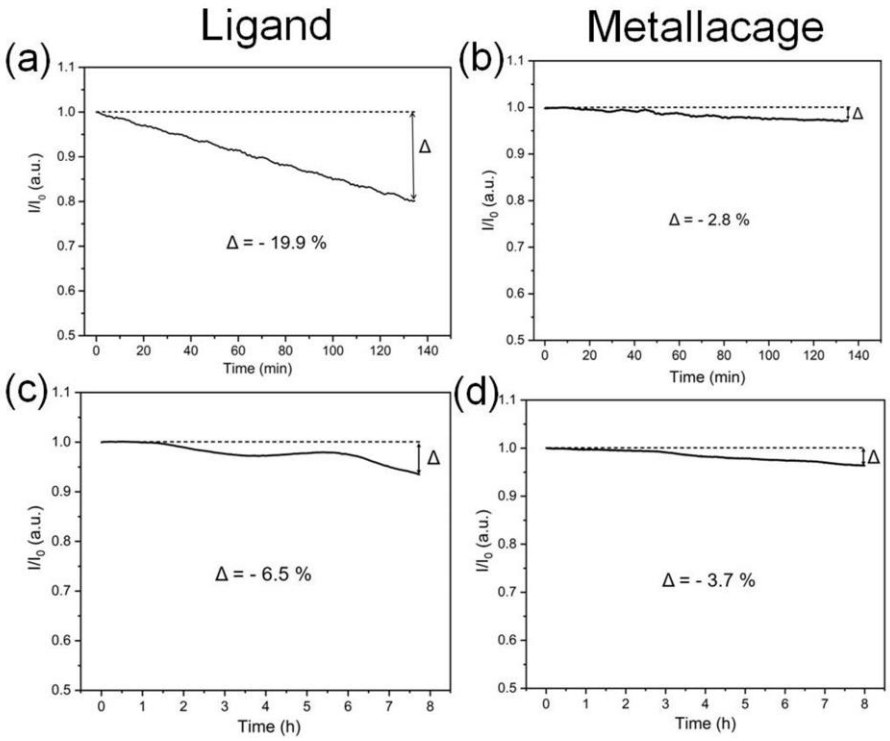

Figure S5. Fluorescence intensity changes of the ligand and the metallacage at the maximum emission wavelength in (a, b) DCM solution and (c, d) film state under 400/430 nm continuous illumination.

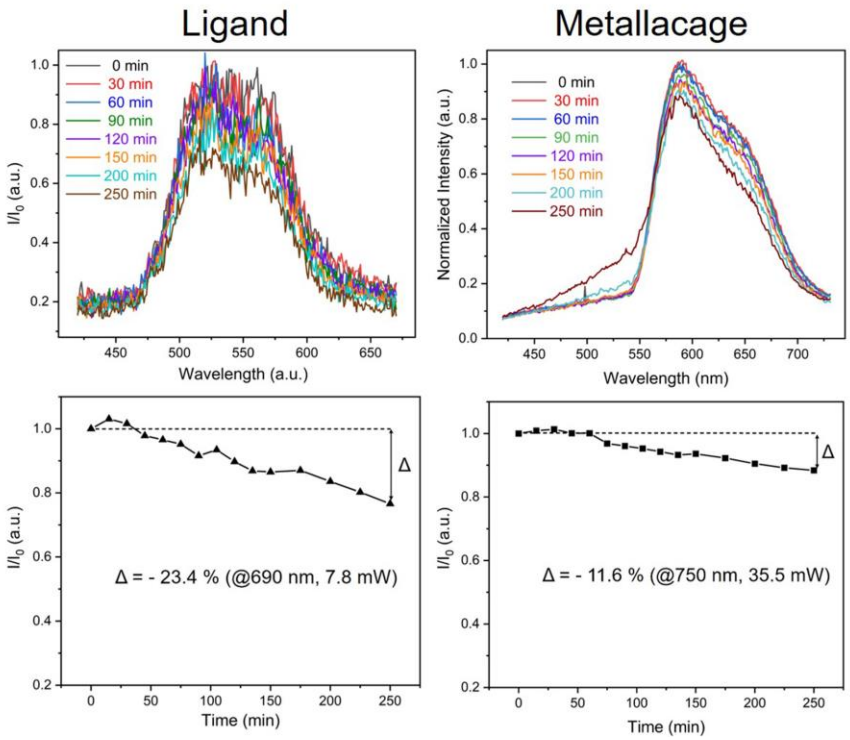

Figure S6. Fluorescence spectra and intensity changes of the ligand and the metallacage at the maximum emission wavelength in DMF solution (1×10^{-2} M) under 7.8 mW 690 nm laser (for the ligand)/35.5 mW 750 nm laser (for the metallacage).

Table S1. Main linear photophysical parameters of the ligand and the metallacage

Comp.	λ_{abs}/nm	ε/M$^{-1}\cdot$cm^{-1}	λ_{em}/nm	$\Delta\lambda$/nm	Φ_F% (silica)	Φ_F% (glass)	τ_F/ns
Ligand	399	6.63×10^4	528	131	1.6	4.4	2.80
Metallacage	437	1.22×10^5	599	162	7.1	7.6	0.93/2.68

Table S2. Main linear photophysical parameters of the ligand and the metallacage in different solvents ($c \approx 1\times10^{-5}$ mol/L). The Φ_F in DMF could not be obtained because the metallacage was not stable in DMF at the same concentration.

The ligand

Solvent	$E_T(30)$	λ_{abs}/nm	λ_{em}/nm	Φ_F%
DCM	40.7	405	506	72.2
Ace	42.2	399	522	55.1
DMF	43.2	404	534	-
MeCN	45.6	398	537	38.7
MeOH	55.4	406	538	2.2

The metallacage

Solvent	$E_T(30)$	λ_{abs}/nm	λ_{em}/nm	Φ_F%
DCM	40.7	455	594	45.1
Ace	42.2	437	599	19.7
DMF	43.2	433	601	-
MeCN	45.6	431	602	21.1
MeOH	55.4	434	590	15.5

4. Crystallographic characterization

Table S3. Crystallographic data and refinement details of the metallacage

Empirical formula	$C_{176}H_{252}F_6N_8O_{18}P_{12}Pt_6S_2$
CCDC Deposit Number	2110646
Formula weight	4488.14
Temperature	193.0 K
Crystal system, space group	Trigonal, P-3
Unit cell dimensions	a = 31.9128(18) Å α = 90 °
	b = 31.9128(18) Å β = 90 °
	c = 17.9523(17) Å γ = 120 °
Volume	15834(2) $Å^3$
Z	2
ρ_{calc}	0.941 $g \cdot cm^3$
Absorption coefficient	3.992 mm^{-1}
F(000)	4484.0
Crystal size	0.12 × 0.1 × 0.1 mm^3
Radiation	GaKα (λ = 1.34139)
2Θ range for data collection/°	2.782 to 121.828
Index ranges	$-28 \leq h \leq 41$, $-41 \leq k \leq 40$, $-17 \leq l \leq 23$
Reflections collected	84333
Independent reflections	22604 [R_{int} = 0.0604, R_{sigma} = 0.0576]
Data/restraints/parameters	22604/281/695
Goodness-of-fit on F^2	0.986
Final R indexes [I>=2σ (I)]	R_1 = 0.0695, wR_2 =0.2303
Final R indexes [all data]	R_1 = 0.1089, wR_2 =0.2590
Largest diff. peak/hole	1.34/-1.54 e $Å^{-3}$

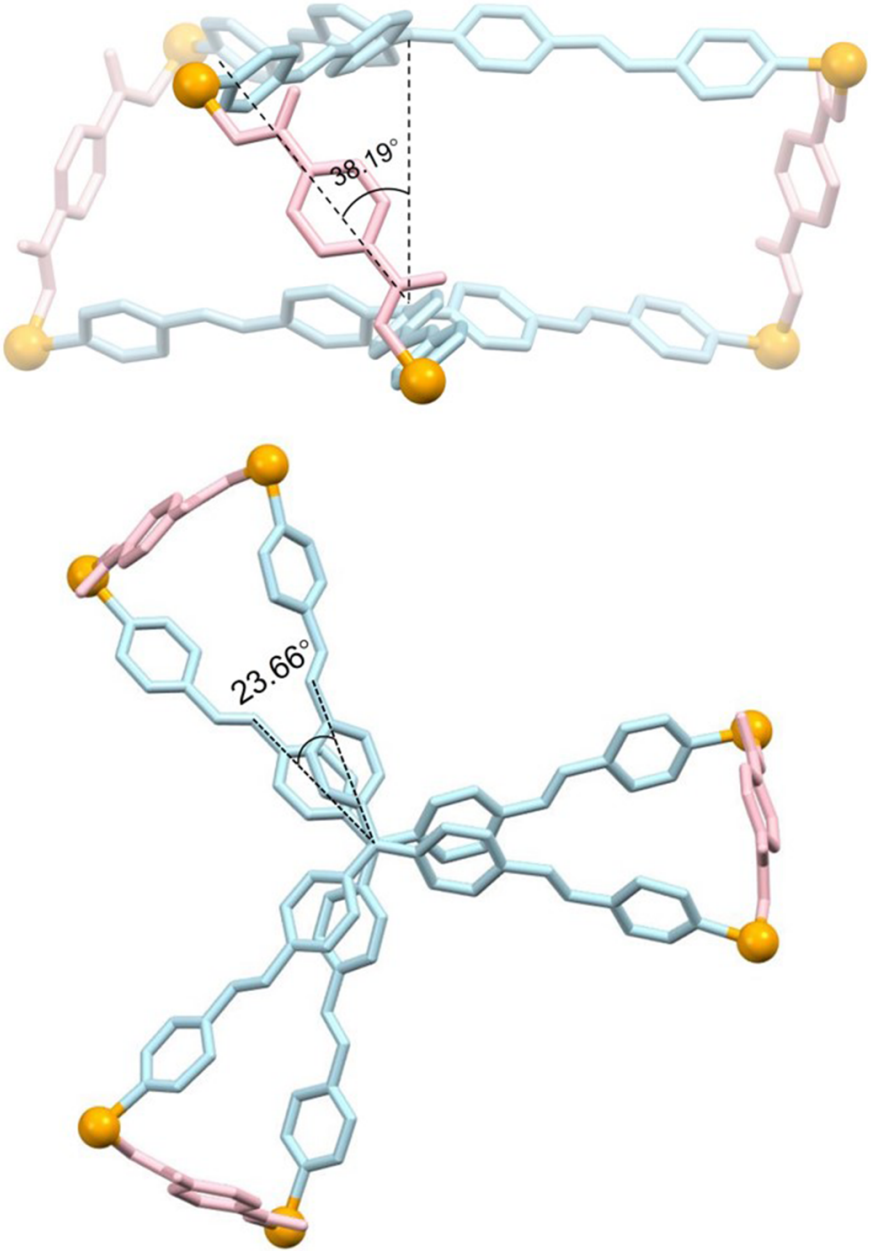

Figure S7. Side and top-on views of the solid-state superstructure of the metallacage with the measurement of deviation angle.

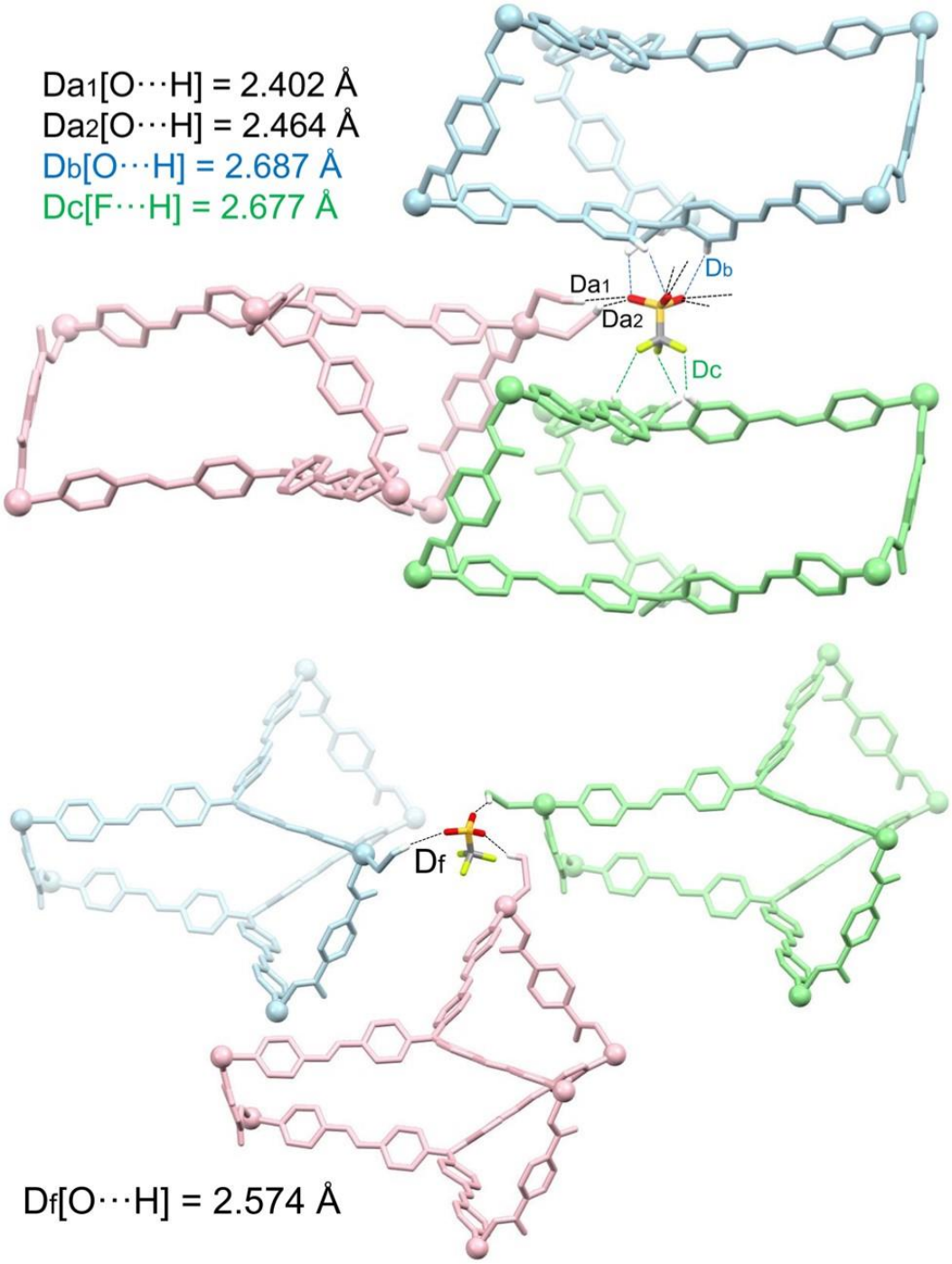

Figure S8. Supramolecular interaction distances of two types of $^{-}$OTf with adjacent metallacages (top for type I and bottom for type II).

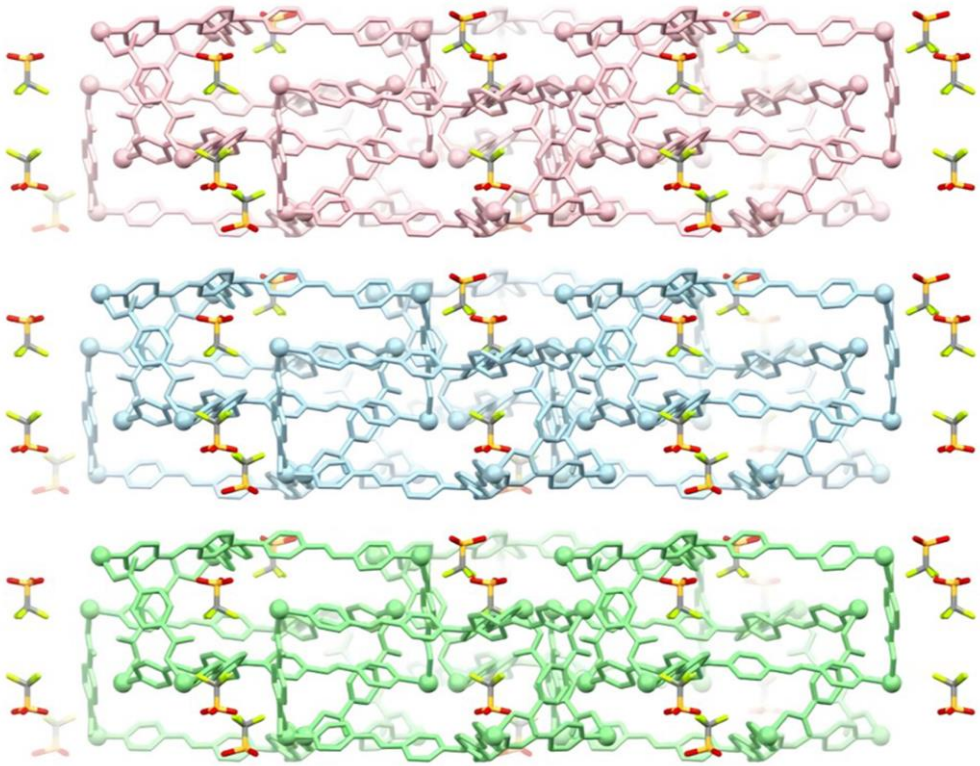

Figure S9. Interlayer packing of the supramolecular structure of the metallacage.

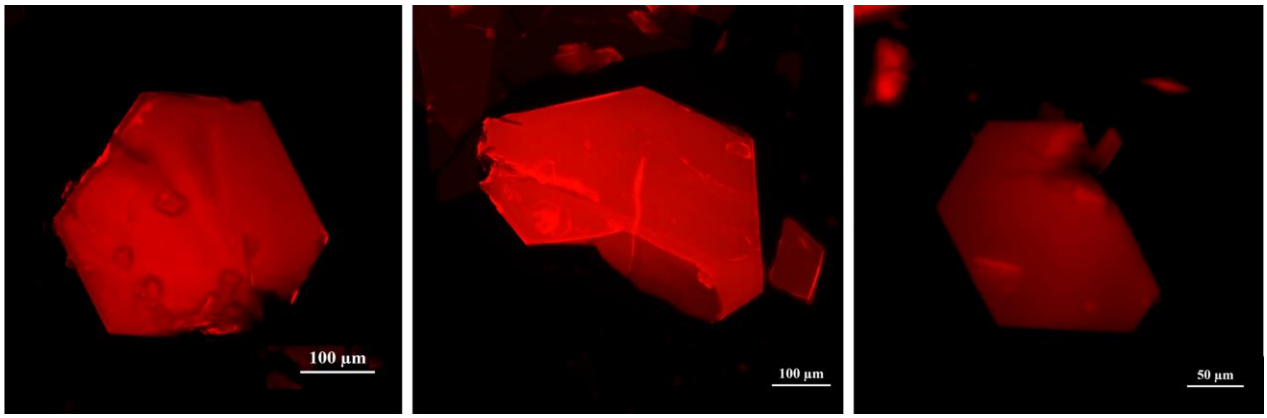

Figure S10. Photographs of solid crystals of the metallcage under UV light.

5. Theoretical calculation data

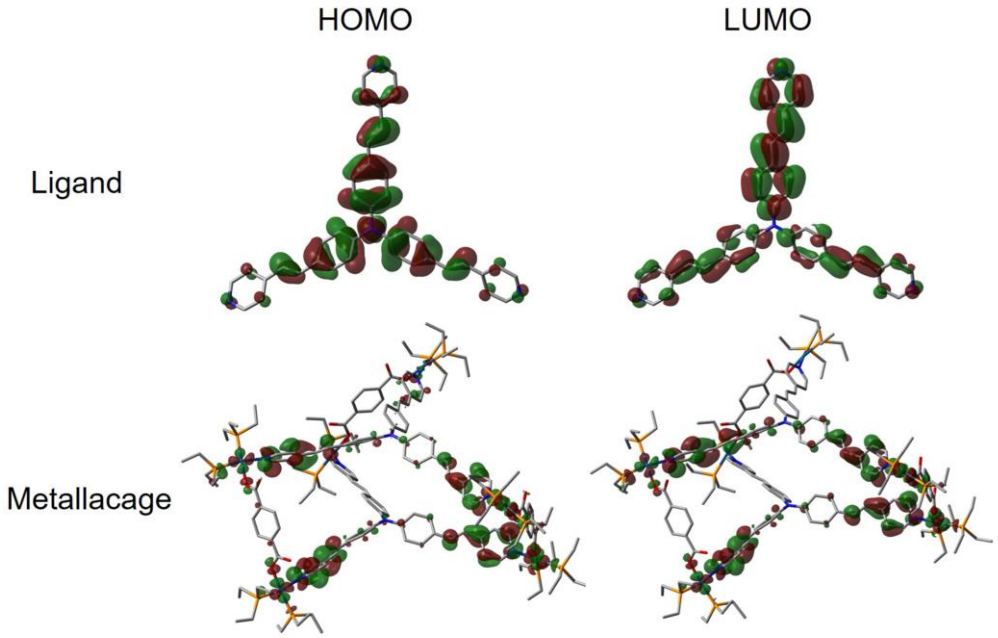

Figure S11. Frontier molecular orbitals at the B3LYP/6-31G(d) level, HOMO and LUMO distribution of the ligand and the metallacage.

Table S4. Excited states, transitions, energy, excitation wavelength and oscillator strength of the ligand

Excited State	Symmetry	Transitions	Energy (eV)	Excitation Wavelength	Osc. Strength (*f*)
1	Singlet-A	HOMO→LUMO	3.1592	392.46	1.3892
2	Singlet-A	HOMO→LUMO+5	3.4093	363.67	1.5606
3	Singlet-A	HOMO→LUMO+2	4.1581	298.17	0.0039
4	Singlet-A	HOMO→LUMO+3	4.2582	291.16	0.0285
5	Singlet-A	HOMO→LUMO+2	4.4650	277.68	0.2420
6	Singlet-A	HOMO-3→LUMO+1	4.6490	266.69	0.6114
7	Singlet-A	HOMO-2→LUMO+1	4.7014	263.72	0.1135
8	Singlet-A	HOMO-4→LUMO	4.7067	263.42	0.0026

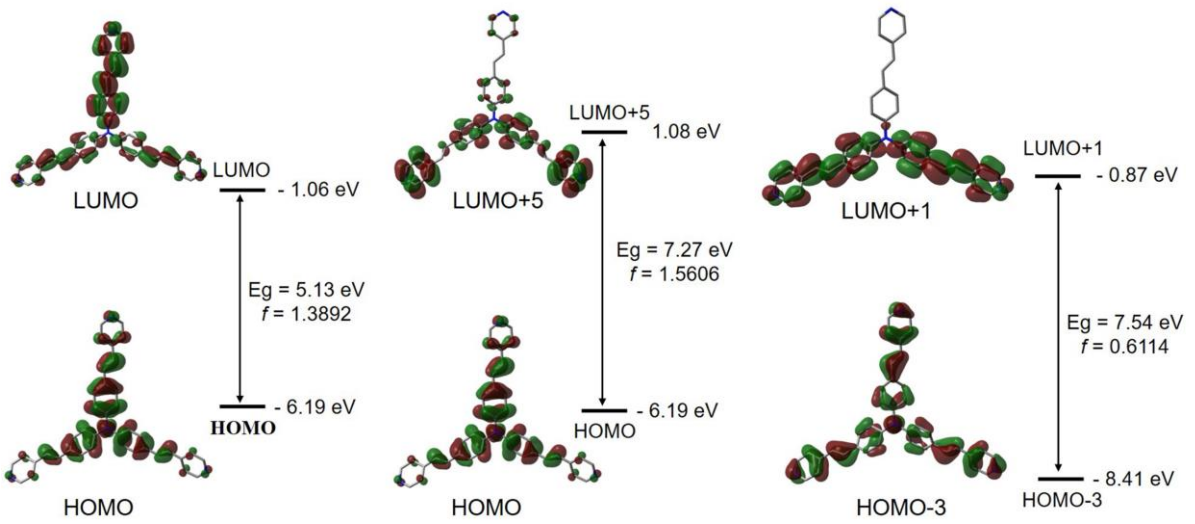

Figure S12. Frontier molecular orbitals, energy gap and the oscillator strength *f* at the B3LYP/6-31G(d) level of the ligand.

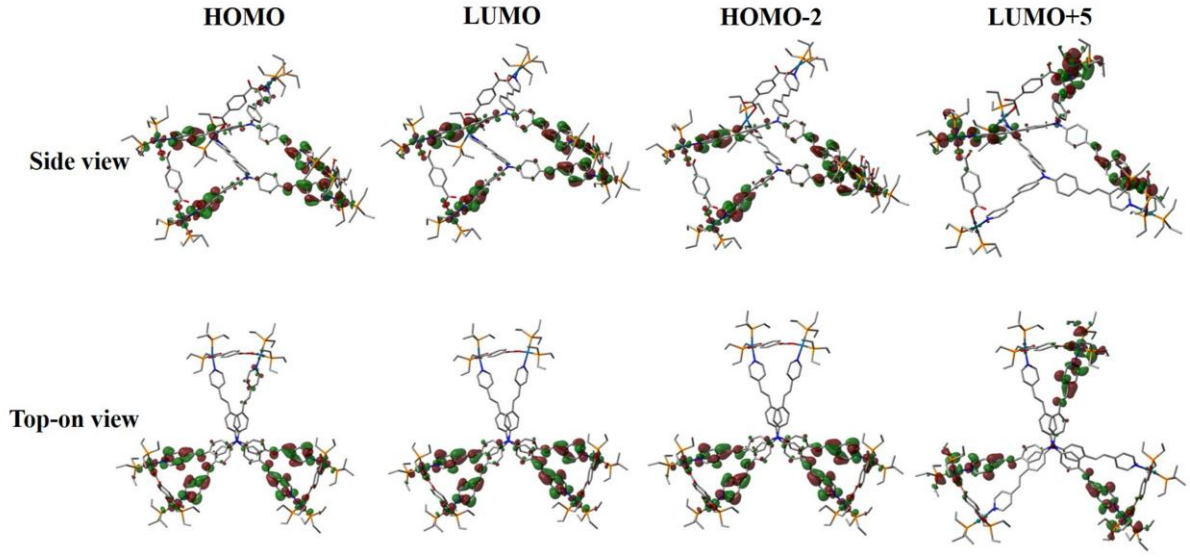

Figure S13. Frontier molecular orbitals of the metallacage in excited states. Calculated at the M06-2X/ 6-31G (d)/ LANL2DZ (for Pt) level.

6. Nonlinear photophysical properties

Table S5. Main nonlinear photophysical parameters of the ligand and the metallacage in DMF (c = 1.0×10^{-2} M)

Comp.	λ_{abs}/nm (1PA)	λ_{abs}/nm (2PA)	β/cm/GW	δ_{2PA}/GM	n_2 /cm^2/GW
Ligand	403	690	0.18	841	8.0×10^{-6}
Metallacage	433	750	0.44	2010	1.8×10^{-5}

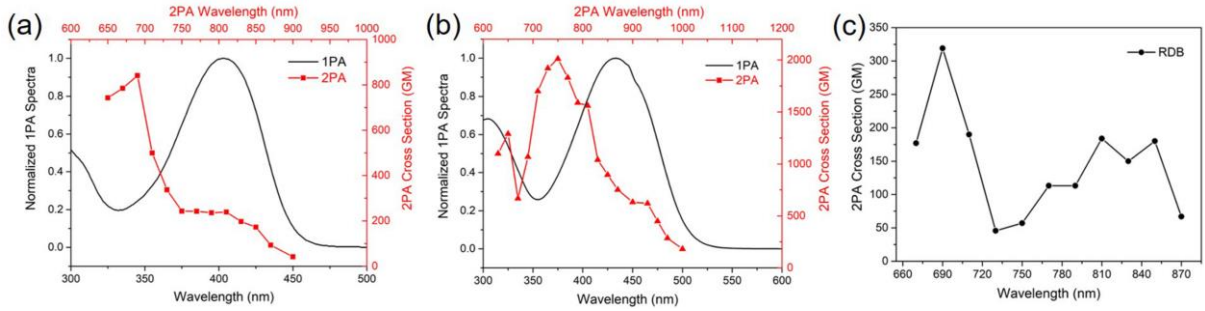

Figure S14. Combined 1PA and 2PA spectra of the ligand (a) and the metallacage (b) in DMF. (c) Two-photon absorption cross section (δ_{2PA}) of the reference compound Rhodamine B (RDB) in DMF excited with different femtosecond wavelengths. (c = 1×10^{-2} M)

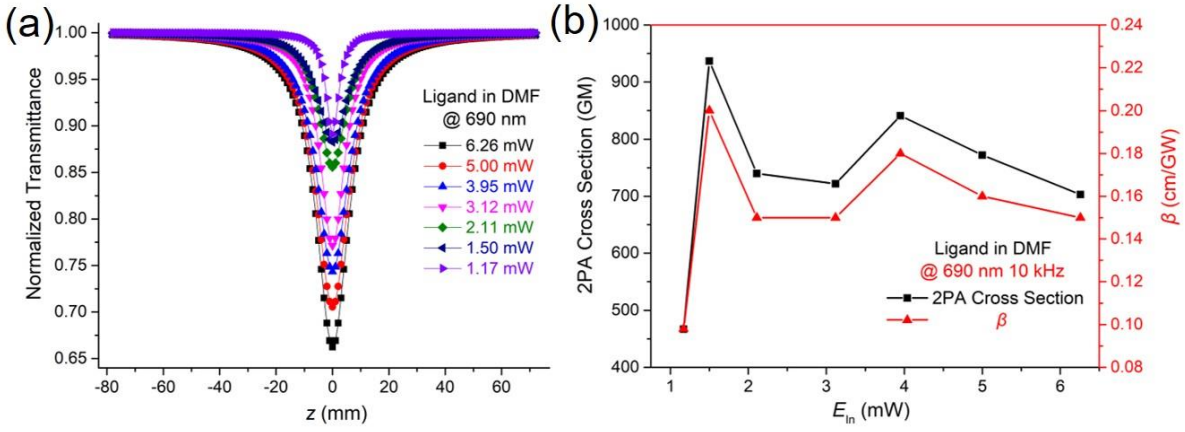

Figure S15. (a) Normalized transmittance curves of the ligand in DMF excited at 690 nm on open aperture Z-scan style with increasing the exciting laser power. (b) δ_{2PA} values and the 2PA coefficient β of the ligand in DMF measured at 690 nm as a function of the input laser power at the focal plane. (c = 1×10^{-2} M)

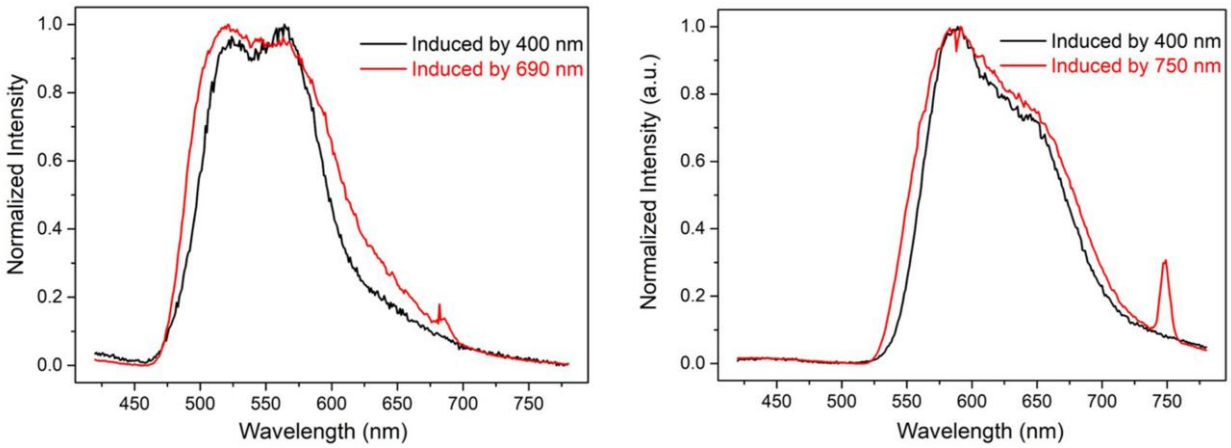

Figure S16. One-photon excited fluorescence and two-photon excited fluorescence (TPEF) spectra of the ligand (left) and the metallacage (right).

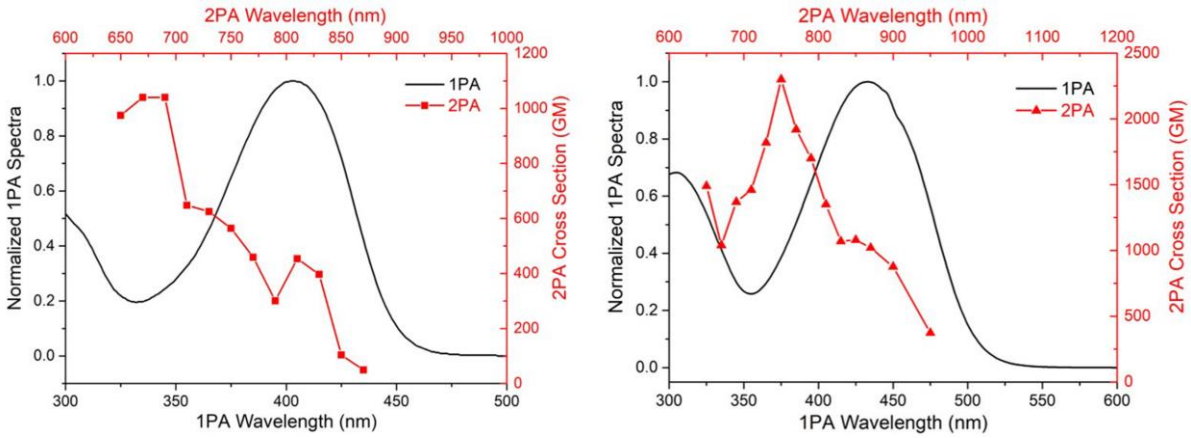

Figure S17. Combined 1PA and 2PA spectra of the ligand (left) and the metallacage (right) in DMF. (c = 2×10^{-3} M)

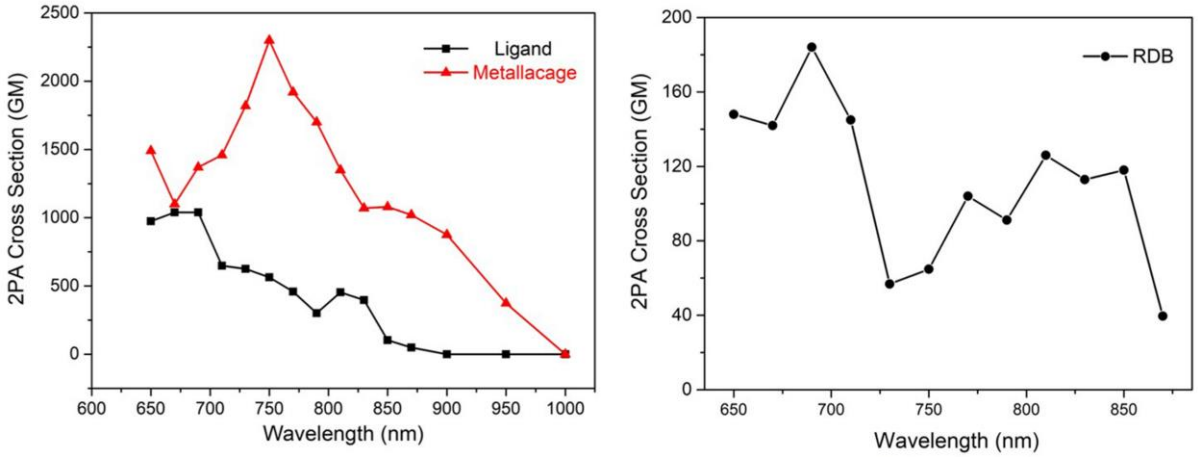

Figure S18. Two-photon absorption cross section (δ_{2PA}) of the ligand and the metallacage (left) (c = 2 × 10^{-3} M) and the reference compound RDB (c = 1 × 10^{-2} M) in DMF excited with different femtosecond wavelengths.

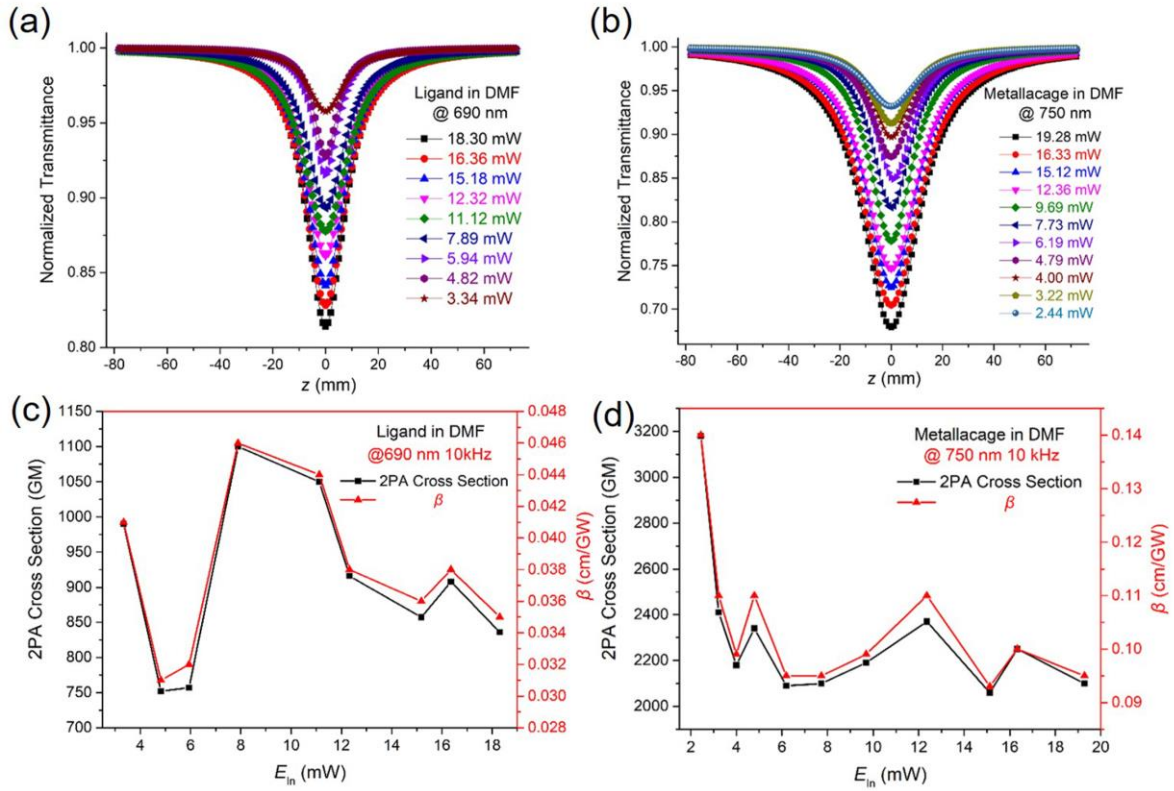

Figure S19. Normalized transmittance curves of the ligand (a) and the metallacage (b) in DMF excited at 690/750 nm on open aperture Z-scan style with increasing the exciting laser power. δ_{2PA} values and the 2PA coefficient β of the ligand (c) and the metallacage (d) in DMF measured at 690/750 nm as a function of the input laser power at the focal plane. (c = 2 × 10^{-3} M)

Table S6. Main nonlinear photophysical parameters of the ligand and the metallacage in DMF (c = 2.0×10^{-3} M)

Comp.	λ_{abs}/nm (1PA)	λ_{abs}/nm (2PA)	β/cm/GW	δ_{2PA}/GM	n_2 /cm^2/GW
Ligand	403	690	0.043	2300	3.6×10^{-6}
Metallacage	433	750	0.10	1040	5.1×10^{-7}

7. NMR and MS characterization data

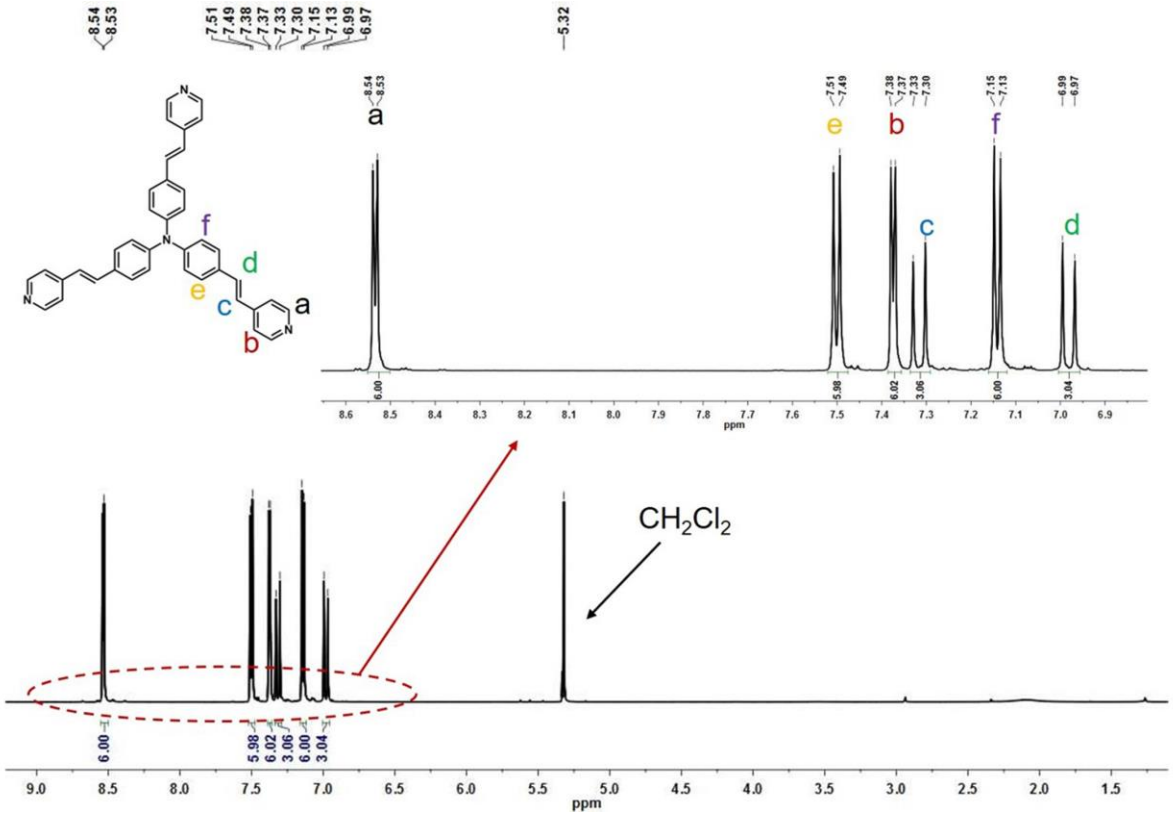

Figure S20. ^{1}H NMR spectrum of the ligand. (600 MHz, CD_2Cl_2, 298 K)

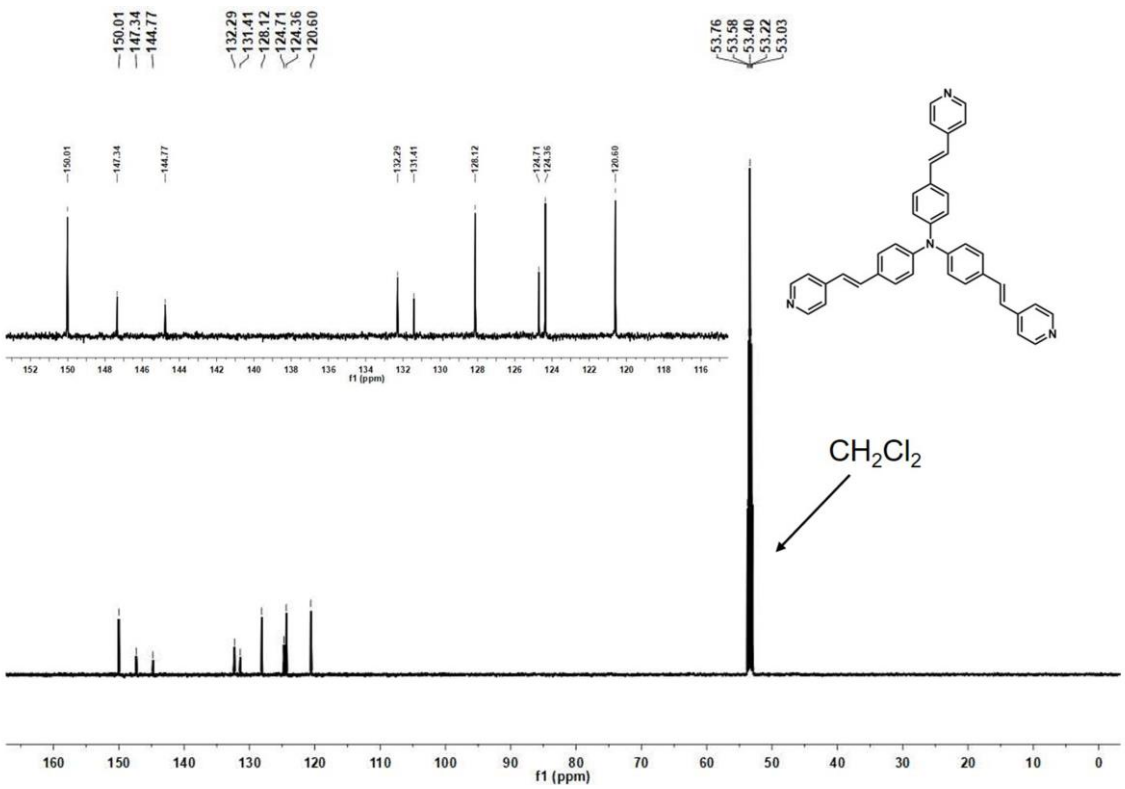

Figure S21. ^{13}C NMR spectrum of the ligand. (151 MHz, CD_2Cl_2, 298 K)

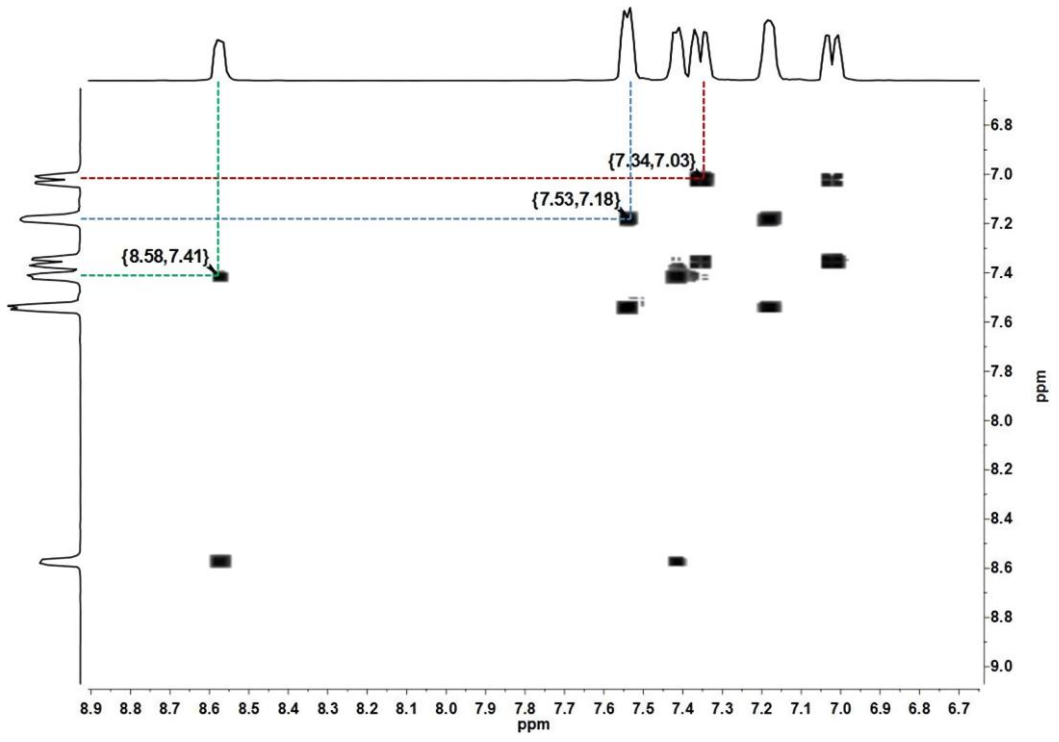

Figure S22. Partial ^{1}H-^{1}H COSY NMR spectrum of the ligand. (600 MHz, CD_2Cl_2, 298 K)

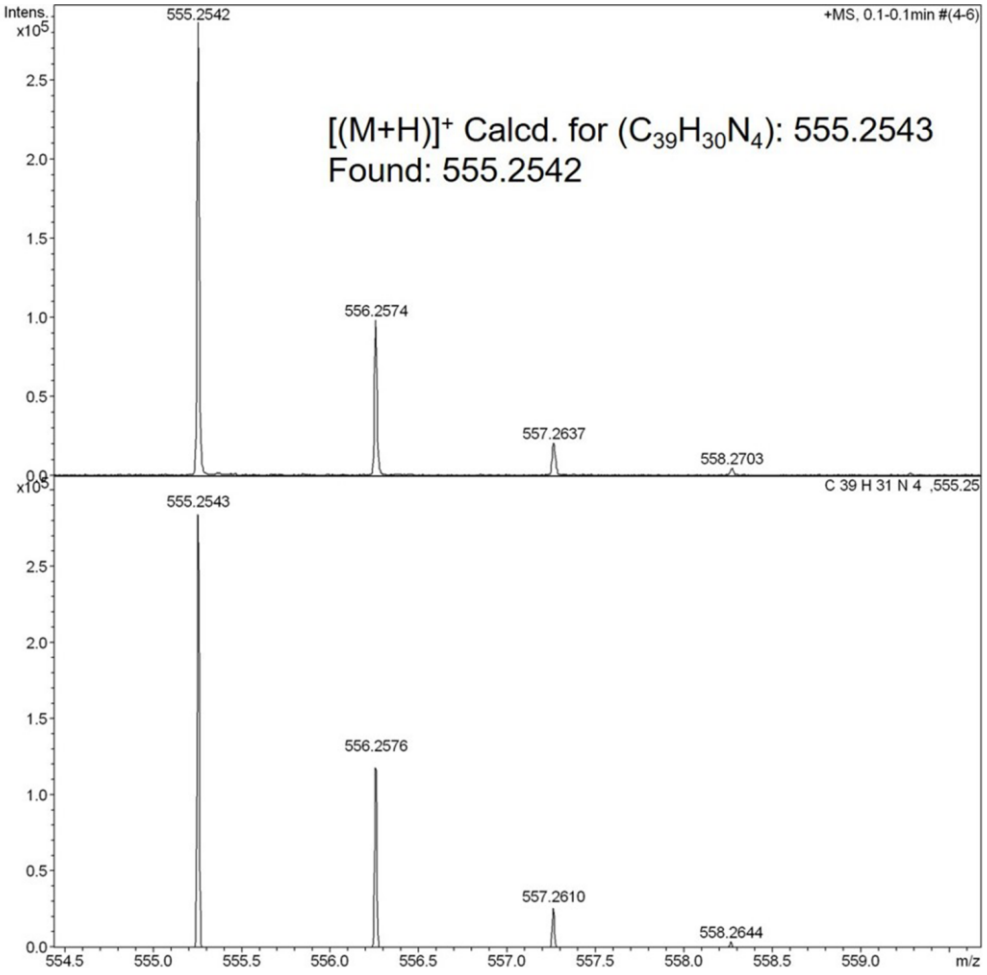

Figure S23. MS spectrum of the ligand. (Top, experimental data; Bottom, theoretical data)

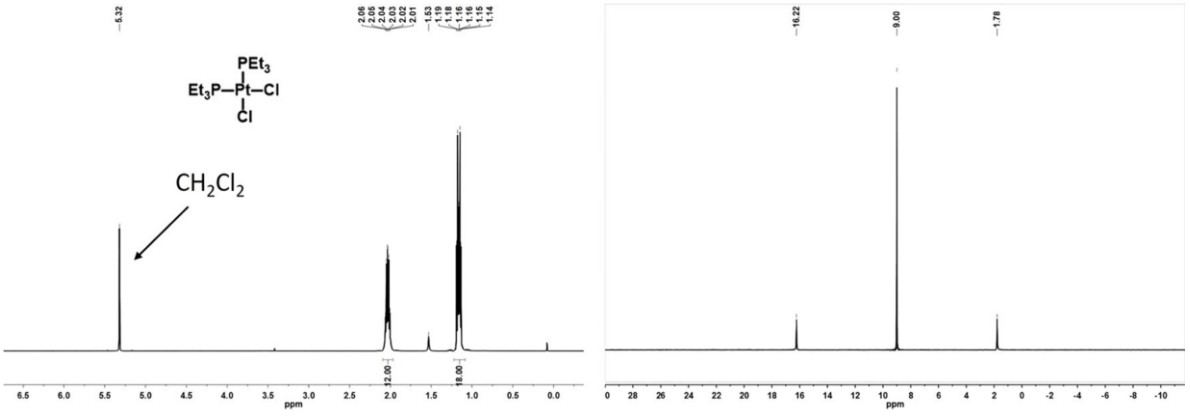

Figure S24. ^{1}H NMR and $^{31}P\{^{1}H\}$ NMR spectra of $PtCl_2(PEt_3)_2$. (600 MHz and 243 MHz, CD_2Cl_2, 298 K)

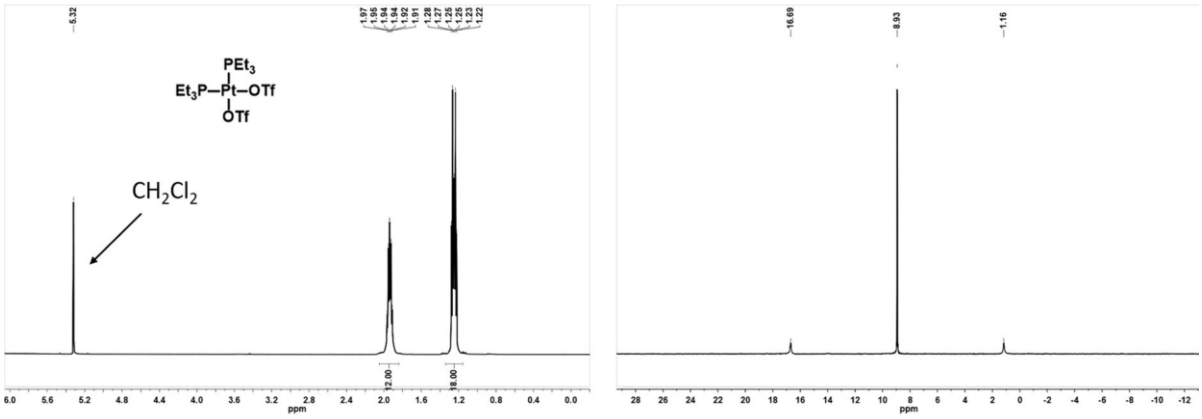

Figure S25. ^{1}H NMR and $^{31}P\{^{1}H\}$ NMR spectra of *cis*-$(PEt_3)_2Pt(OTf)_2$.(600 MHz and 243 MHz, CD_2Cl_2, 298 K)

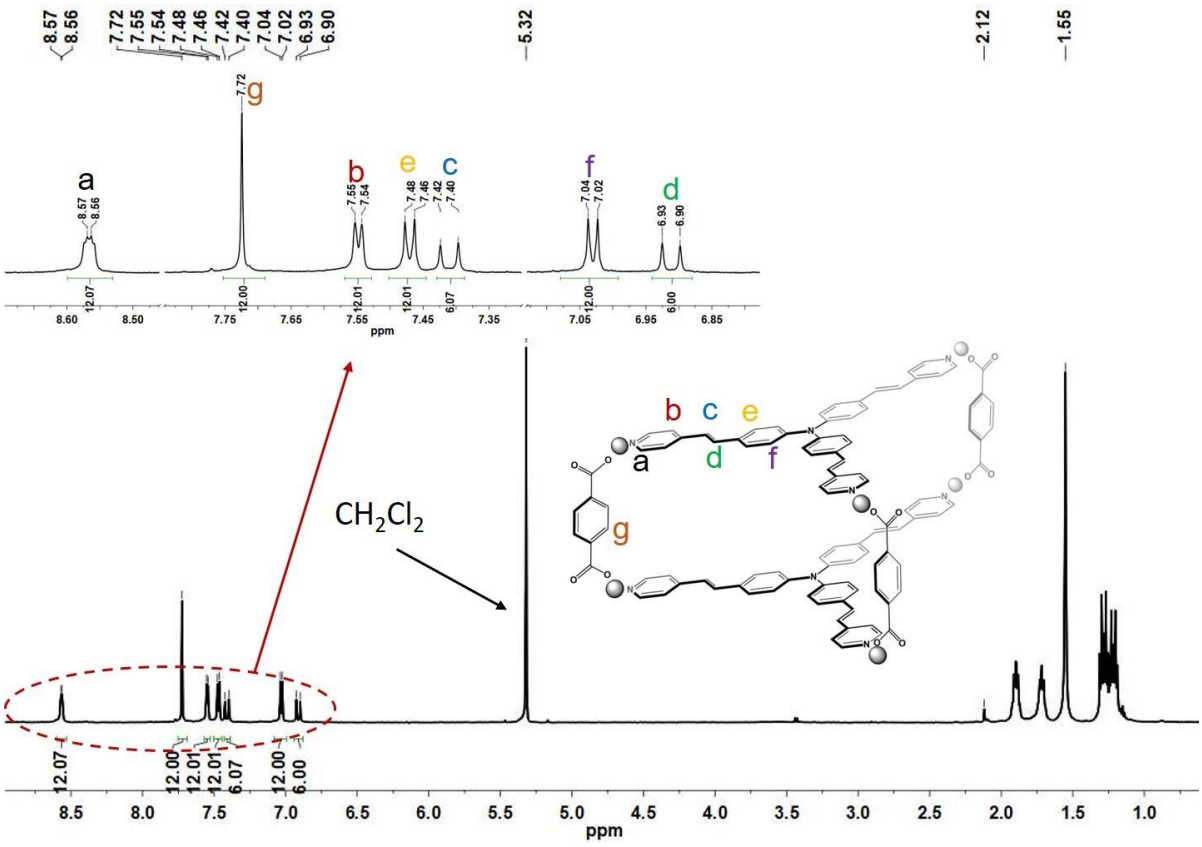

Figure S26. ^{1}H NMR spectrum of the metallacage. (600 MHz, CD_2Cl_2, 298 K)

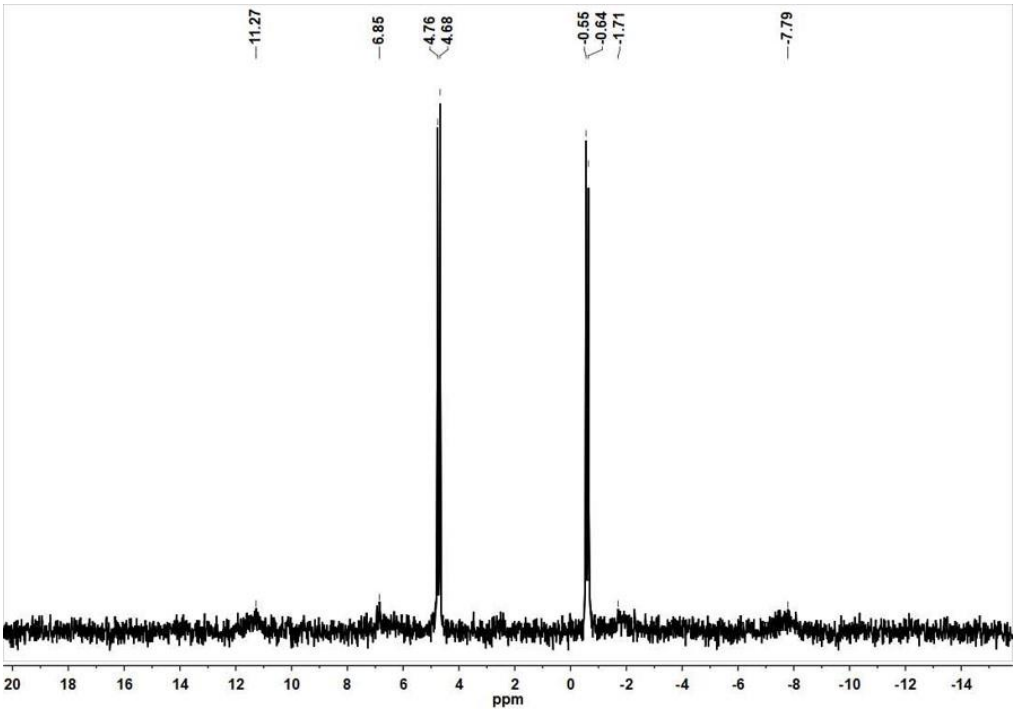

Figure S27. $^{31}P\{^{1}H\}$ NMR spectrum of the metallacage. (243 MHz, CD_2Cl_2, 298 K)

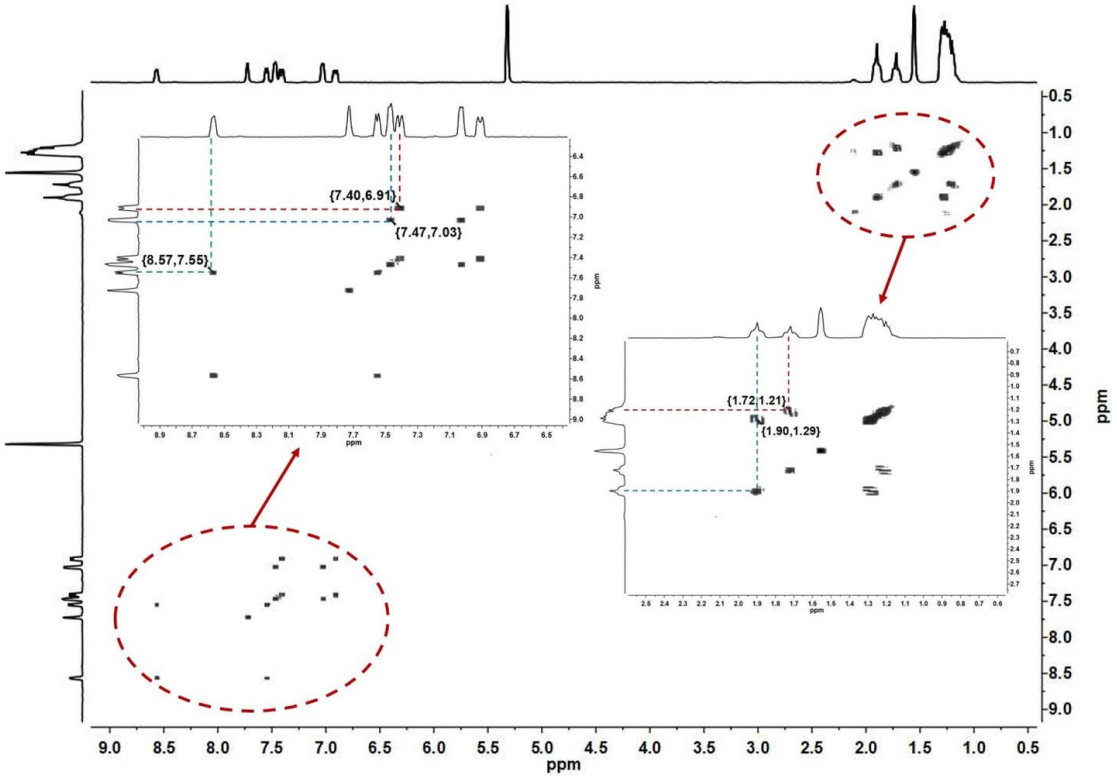

Figure S28. ^{1}H-^{1}H COSY NMR spectrum of the metallacage. (600 MHz, CD_2Cl_2, 298 K)

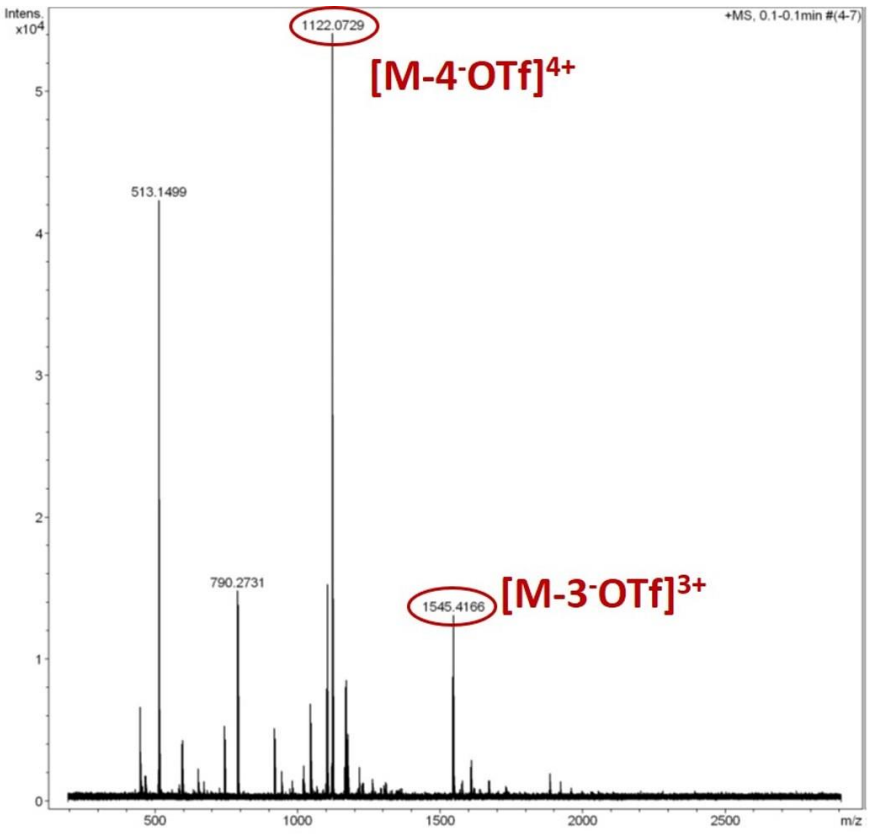

Figure S29. ESI-TOF-MS spectrum of the metallacage.

References

[1] Sheik-bahae, M.; Said, A. A.; Van Stryland, E. W. High-Sensitivity, Single-Beam n_2 Measurements. *Opt. Lett.* **1989**, *14*, 955-957.

[2] Sheik-bahae, M.; Said, A. A.; Wei, T.-H.; Hgan, D. J.; Van Stryland, E. W. *IEEE J. Quantum Electron.* **1990**, *26*, 760-769.

[3] Makarov, N. S.; Drobizhev, M.; Rebane, A. Two-photon Absorption Standards in the 550-1600 nm Excitation Wavelength Range. *Opt. Express* **2008**, *16*, 4029-4047.

[4] Ajami, A.; Husinsky, W.; Ovsianikov, A.; Liska, R. Dispersive White Light Continuum Single Z-scan for Rapid Determination of Degenerate Two-Photon Absorption Spectra. *Appl. Phys. B* **2018**, *124*, 142.

[5] Zang, J.; Feng, W.; Chang, X.; Liu, K.; Peng, H.; Ding, L.; Liu, T.; Fang, Y. Enhanced Two-Photon Absorption of Sandwich-Like Coordination Complexes Based on Squaraine and Metallomacrocycle Derivatives. *Dyes Pigm.* **2021**, *193*, 109487.

[6] Feng, W.; Liu, K.; Zang, J.; Xu, J.; Peng, H.; Ding, L.; Liu, T.; Fang, Y. Resonance- Enhanced Two-Photon Absorption and Optical Power Limiting Properties of Three-Dimensional Perylene Bisimide Derivatives. *J. Phys. Chem. B* **2021**, *125* (41), 11540-11547.